Progress of Theoretical Physics, Vol. 75, No. 5, May 1986

Stability Theory of Synchronized Motion in Coupled-Oscillator Systems. IV

—— *Instability of Synchronized Chaos and New Intermittency* ——

Hirokazu FUJISAKA and Tomoji YAMADA*

Department of Physics, Kagoshima University, Kagoshima 890
**Department of Physics, Kyushu Institute of Technology, Kitakyushu 804*

(Received November 25, 1985)

A coupled-chaos system consisting of two subsystems, which is also derived by the three mode truncation in a spatially continuous system, is studied immediately after the instability point of the synchronized chaos. The system turns out to exhibit two types of intermittency, one is similar to the tangential type and the other in a new one, depending on the fluctuation characteristics of local expansion rates of adjacent trajectories in the synchronized chaos. In the new intermittency, the temporal evolution of the difference between state variables is characterized by quiescent regions abruptly inserted by bursts which are temporally highly localized. Its probability density is found to obey approximately an inverse power law, and its power spectrum is observed to exhibit the ω^{-1} law in a certain low frequency region.

§ 1. Introduction

In a series of papers,[1)~3)] we have studied the stability of the synchronized motion in coupled-oscillator systems, especially of the diffusion type coupling. Particularly, when the uncoupled oscillator is chaotic, the coupled system undergoes the transition as the coupling strength is decreased (see I and II). Furthermore, as was reported in II and III, when the uncoupled system has a one dimensional map, the coupled-oscillator system can be described by the coupled-map system.

Consider one oscillator system under the external periodic excitation with the period T_e,

$$\dot{\boldsymbol{x}}(t)=\boldsymbol{F}(\boldsymbol{x};\, t)\,, \tag{1·1}$$

where $\boldsymbol{x}(t)$ is the state vector at the time t and satisfies $\boldsymbol{F}(\boldsymbol{x};\, t+T_e)=\boldsymbol{F}(\boldsymbol{x};\, t)$. We assume that by ignoring a fractal structure (1·1) has one dimensional stroboscopic map, for a certain component $x(t)$ of $\boldsymbol{x}(t)$,

$$x_{n+1}=f(x_n)\,, \tag{1·2}$$

where $x_n=x(t_n)$, $t_n=nT$,$(n=0, 1, 2, \cdots)$, T being a certain integer multiple of T_e.[2)]

Suppose that oscillators each of which is described by (1·1) are contained in a d-dimensional space and are coupled to each other as follows,

$$\dot{\boldsymbol{x}}(\boldsymbol{\xi}, t)=\boldsymbol{F}(\boldsymbol{x}(\boldsymbol{\xi}, t);\, t)+\boldsymbol{C}(\boldsymbol{x}(\boldsymbol{\xi}, t);\, \{\boldsymbol{x}(\boldsymbol{\xi}', t)\})\,, \tag{1·3}$$

where $\boldsymbol{x}(\boldsymbol{\xi}, t)$ is the state vector at the position $\boldsymbol{\xi}$ at the time t. $\boldsymbol{C}$ denotes the coupling term, being assumed to be autonomous, and is chosen in such a way that (1·3) has a spatially uniform oscillation $\dot{\boldsymbol{x}}^0=\boldsymbol{F}(\boldsymbol{x}^0;\, t)$, $\boldsymbol{x}^0$ being independent of $\boldsymbol{\xi}$. This state will be called the *synchronized state* Ψ_{unif}. Let us assume that if $\boldsymbol{C}$ is suitably chosen, then (1·3) is reduced to the following coupled-map system

$$x_{n+1}(\xi)=\int\phi(|\xi-\xi'|)f(x_n(\xi'))\,d\xi' \tag{1·4}$$

or equivalently,

$$x_{n+1}(\xi)=\hat{\phi}_{-i\nabla}f(x_n(\xi))\,,\quad(\nabla\equiv\partial/\partial\xi) \tag{1·5}$$

where $x_n(\xi)\equiv x(\xi, t_n)$ and $f(x)$ is the same as in (1·2). The kernel $\phi(|\xi|)$ depends only on $|\xi|$ and measures the interaction strength among oscillators at different positions. The $\hat{\phi}_k$ has been introduced by

$$\hat{\phi}_k\equiv\int\phi(|\xi|)\,e^{-ik\cdot\xi}d\xi\,. \tag{1·6}$$

Since the system (1·3) has the synchronized state, (1·4) should also have the synchronized state obeying $x^0_{n+1}=f(x_n{}^0)$. This requirement leads to

$$\int\phi(|\xi|)\,d\xi=\hat{\phi}_0=1\,. \tag{1·7}$$

Furthermore, in order that $x_n(\xi)$ is always bounded, we impose the condition

$$\phi(|\xi|)\geqq 0\,. \tag{1·8}^{*)}$$

Hereafter $\hat{\phi}_k$ is assumed to go to zero as $|k|$ is increased (Appendix A).

Particularly, consider a system with[3]

$$\dot{\boldsymbol{x}}=C\nabla^2\boldsymbol{x}(\xi, t)\,.\qquad(C>0) \tag{1·9}$$

Since (1·3) and (1·4) should have the same stability exponent Λ_k (Eq. (A·4)) for the wavenumber k, $\hat{\phi}_k$ should have the Gaussian

$$\hat{\phi}_k=\exp(-\alpha k^2) \tag{1·10}$$

with $\alpha=CT$. Accordingly we obtain[3]

$$x_{n+1}(\xi)=\exp(\alpha\nabla^2)f(x_n(\xi))\,. \tag{1·11}$$

This is the same result as that derived in III. Turning to (1·4), we find that the interaction kernel is given by the Gaussian

$$\phi(\xi)=(4\pi\alpha)^{-d/2}\exp\left(-\frac{\xi^2}{4\alpha}\right) \tag{1·12}$$

for an infinitely large system. So the oscillator at the position ξ is affected by oscillators being in the range $|\xi'-\xi|\lesssim 2\sqrt{\alpha}$. If the coupling strength α is small, oscillators behave rather independently, and if α is large, oscillators in a wide range affect to each other.

Next we consider the two-oscillator system[1),2)]

$$\dot{\boldsymbol{x}}^{(j)}(t)=\boldsymbol{F}(\boldsymbol{x}^{(j)};\,t)+(C/2)\sum_{l=1}^{2}(\boldsymbol{x}^{(l)}-\boldsymbol{x}^{(j)})\,,\qquad(j=1, 2) \tag{1·13}$$

where $C(>0)$ is the coupling strength. The mapping system corresponding to (1·13) is

*) Suppose that x_n obeying (1·2) is bounded, $x_{\min}\leqq x_n\leqq x_{\max}$, and so $x_{\min}\leqq f(x_n)\leqq x_{\max}$. If (1·8) holds, then Min $x_{n+1}(\xi)=\int d\xi'\,\phi(|\xi-\xi'|)\times$Min $f(x_n(\xi'))\geqq x_{\min}$ and Max $x_{n+1}(\xi)=\int d\xi'\,\phi(|\xi-\xi'|)$Max $f(x_n(\xi'))\leqq x_{\max}$, where we have used (1·7). Therefore $x_n(\xi)$ obeying (1·4) is always in the region $x_{\min}\leqq x_n(\xi)\leqq x_{\max}$.

rewritten as[2),4)]

$$x_{n+1}^{(j)}=\sum_{l=1}^{2}\phi_{jl}f(x_n^{(l)}), \qquad (j=1,2) \tag{1·14}$$*)

where $x_n^{(j)}\equiv x^{(j)}(t_n)$. The oscillator symmetry enables us to put[2)]

$$\{\phi_{jl}\}=\begin{pmatrix}1-\phi & \phi\\ \phi & 1-\phi\end{pmatrix}, \tag{1·15}$$

which satisfies $\sum_{l=1}^{2}\phi_{jl}=1$, corresponding to (1·7). Furthermore, (1·13) and (1·14) with (1·15) should give the same stability condition on Ψ_{unif}. This leads to the replacement[2)]

$$\phi=(1-e^{-\alpha})/2, \quad (0<\phi<1/2) \tag{1·16}$$

where $\alpha=CT$. This is the same as in II. We note that the systems (1·13) and (1·14) have the synchronized state, independently of the coupling strength C. As was shown previously,[2)] (1·14) with (1·15) and (1·16) reproduces the statistical characteristics of the original system (1·13) surprizingly well both qualitatively and quantitatively for any C.

Hereafter we assume that (1·1) exhibits chaos, so (1·2) has a positive Lyapunov exponent. Accordingly, Ψ_{unif} of (1·3) and (1·13) should also be chaotic. As will be discussed in Appendix A, when the uniform chaos is suitably weak so that the statistical behaviors of the coupled system can be described by the three mode truncation, the extended map (1·4) or (1·5) can be approximated by (1·14).

The main aims of the present paper are to develop a stability theory on Ψ_{unif} of (1·14), and to study statistical properties of the system slightly below the instability point of Ψ_{unif}. In carrying out numerical calculations, it is convenient to rewrite (1·14) as follows. By introducing

$$\bar{x}_n=(x_n^{(1)}+x_n^{(2)})/2, \tag{1·17a}$$

$$v_n=(x_n^{(1)}-x_n^{(2)})/2, \qquad r_n=|v_n| \tag{1·17b}$$

(1·14) becomes

$$\bar{x}_{n+1}=f(\bar{x}_n)+g(\bar{x}_n, v_n), \tag{1·18}$$

$$v_{n+1}=S(\bar{x}_n, v_n)e^{-\alpha}v_n, \tag{1·19}$$

where

$$g(\bar{x}, v)=\{f(\bar{x}+v)+f(\bar{x}-v)-2f(\bar{x})\}/2, \tag{1·20a}$$

$$S(\bar{x}, v)=\{f(\bar{x}+v)-f(\bar{x}-v)\}/2v. \tag{1·20b}$$

Equations (1·18) and (1·19) describe the temporal evolutions of the average motion and the difference between $x_n^{(1)}$ and $x_n^{(2)}$, respectively.

The remaining part of the present paper is constructed as follows. In § 2 we will develop a fluctuation theory on the stability of the synchronized chaos. In §§ 3 and 4, utilizing the logistic parabolla $f(x)=ax(1-x)$, we shall numerically integrate (1·18) and (1·19) for a slightly below a_c, the instability point of Ψ_{unif}, and will find two types of intermittency. Several statistical characteristics associating with them will be discussed

*) A similar system has been studied in Ref. 5).

in connection with the fluctuation effect of local expansion rates in the synchronized chaos. Summary and remarks are given in § 5.

§ 2. Fluctuation theory on the stability of synchronized chaos

When the system is close to Ψ_{unif}, (1·18) and (1·19) can be expanded around $x_n^{(1)} = x_n^{(2)} \equiv x_n^0$. If we retain $O(v_n)$ terms, they become

$$x_{n+1}^0 = f(x_n^0)\,, \tag{2·1}$$

$$v_{n+1} = f'(x_n^0)\,e^{-\alpha} v_n\,. \qquad (f'(x) = df(x)/dx) \tag{2·2}$$

Equation (2·1) describes the evolution of x_n^0 in Ψ_{unif}, and is not concerned with the stability of Ψ_{unif}. Equation (2·2) is, on the other hand, the perturbation equation determining the stability of Ψ_{unif}, and is rewritten as

$$r_{n+1} = \exp(\Lambda_n - \alpha)\, r_n\,. \tag{2·3}$$

Here

$$\Lambda_n = \ln|f'(x_n^0)| \tag{2·4}$$

is the local expansion rate for adjacent trajectories[6] in (2·1). r_n estimates the difference between $x_n^{(1)}$ and $x_n^{(2)}$, (Eq. (1·17b)), when they are close to x_n^0.

Let λ_0 be the Lyapunov exponent of $x_{n+1}^0 = f(x_n^0)$,

$$\lambda_0 = \langle \Lambda_n \rangle = \langle \ln|f'(x_n^0)| \rangle\,, \quad (>0) \tag{2·5}$$

where $\langle \cdots \rangle$ is the ensemble average over the invariant density $\rho(x)$ satisfying $\rho(x) = \int \delta(f(y) - x)\rho(y)\,dy$. Furthermore, let D be the diffusion coefficient in the $\ln r$ space, defined by[6),7)]

$$\begin{aligned} D &= \lim_{n\to\infty} \langle \{\ln(r_n/r_0) - \chi_0 n\}^2 \rangle / 2n \\ &= G_0/2 + \sum_{n=1}^{\infty} G_n\,, \end{aligned} \tag{2·6}$$

where $G_n \equiv \langle \delta\Lambda_n \delta\Lambda_0 \rangle$ $(\delta\Lambda_n \equiv \Lambda_n - \lambda_0)$, is the correlation function of the local expansion rate, and

$$\chi_0 \equiv \lambda_0 - \alpha\,. \tag{2·7}$$

With the assumption that $D = \text{finite} \neq 0$, which is equivalent to that G_n decays faster than $\propto n^{-1}$, the central limit theorem tells us that the probability density $P(z, n)$ for $z_n \equiv \ln(r_n/r_0)$, $(P(z, 0) = \delta(z))$, asymptotically has the Gaussian

$$P(z, n) \simeq \frac{1}{\sqrt{4\pi D n}} \exp\left\{ -\frac{(z - \chi_0 n)^2}{4Dn} \right\} \tag{2·8}$$

for $n \to \infty$. Equivalently the probability density $Q(r, n)$ for r_n itself is given by the lognormal one,

$$Q(r, n) \simeq \frac{r_0}{\sqrt{4\pi D n}\, r} \exp\left[-\frac{\{\ln(r/r_0) - \chi_0 n\}^2}{4Dn} \right] \tag{2·9}$$

for $n\to\infty$.

By noting that almost all probability of z_n is contained in the Gaussian region (2·8), if its peak position tends to $-\infty$ as $n\to\infty$, i.e., if $\varkappa_0<0$, then the system eventually approaches the uniform (synchronized) chaos. On the other hand, for $\varkappa_0>0$, Ψ_{unif} is unstable. Therefore the system undergoes the transition from the uniform chaos to a non-uniform state at

$$\alpha=\alpha_c\equiv\lambda_0\,, \tag{2·10}$$

as the coupling strength α is decreased from a value large enough.[1)~4)] This transition occurs as a result of the counterbalancing between the trajectory instability specified by the positive Lyapunov exponent and the coupling effect.[1),2)]

As far as α is close to α_c, the non-uniformity of the coupled system is small provided that the transition is continuous. Therefore we can expect that for $\alpha\lesssim\alpha_c$ the statistical characteristics reflect certain aspects of the uniform chaos. By noting that the transition point is determined by the average of local expansion rates (Eq. (2·10)), it is natural to study the fluctuation effect of local expansion rates. This is equivalent to studying the fluctuation dynamics of r_n itself in (2·3). If we define

$$l_q(n)\equiv\langle r_n{}^q\rangle^{1/q}=r_0\langle\exp\{q\sum_{j=0}^{n-1}(\Lambda_j-\alpha)\}\rangle^{1/q}\,,\qquad(-\infty<q<\infty) \tag{2·11}$$

it measures the fluctuation of the characteristic difference between $x_n{}^{(1)}$ and $x_n{}^{(2)}$, specified by the power q. $l_0(n)$ $(=\exp(\langle\ln r_n\rangle))=r_0\exp(\varkappa_0 n)$ is the difference when we neglect the fluctuation of Λ_n from λ_0. $l_1(n)$ is the usual average difference, $l_2(n)$ is the root mean square difference and $l_3(n)$ is the root mean cube difference and so on.

In order to discuss the long time dynamics of r_n, it is convenient to rewrite (2·11) as

$$l_q(n)=r_0A_q(n)\exp(\varkappa_q n)\,. \tag{2·12}$$

Here $\varkappa_q$ is given by

$$\varkappa_q=\lambda_q-\alpha\,, \tag{2·13}$$

where

$$\lambda_q\equiv q^{-1}\lim_{n\to\infty}n^{-1}\ln\langle\exp(q\sum_{j=0}^{n-1}\Lambda_j)\rangle\,,\qquad(d\lambda_q/dq\geqq 0) \tag{2·14}$$

is the q-order similarity exponent[7),*)] for fluctuations of local expansion rates of $x_{n+1}^0=f(x_n{}^0)$, and is completely determined by the statistical property in Ψ_{unif}. Particularly, for $q=0$ (2·14) is identical to the Lyapunov exponent defined in (2·5), and (2·13) reduces to (2·7). $A_q(n)$ is independent of r_0 and satisfies $\lim_{n\to\infty}n^{-1}\ln A_q(n)=0$. So the most dominant contribution to $l_q(n)$ in a long time is determined by $\varkappa_q$.

First consider a special case where λ_q has no dispersion,[**)] i.e.,

$$\lambda_q=\lambda_0 \tag{2·15}$$

for any q. In this case there exists only one characteristic difference

*) The similarity exponent for fluctuations of local expansion rates is invariant under a one-to-one transformation $\tilde{x}_n=h(x_n)$.[7)] For $q\to 0$, λ_q can be expanded as $\lambda_q=\lambda_0+Dq+O(q^2)$, where D is the diffusion coefficient defined by (2·6). If $x_n{}^0$ is periodic, λ_q has no dispersion ($\lambda_q=\lambda_0<0$).

**) If the local expansion rate Λ_n is everywhere λ_0, we immediately get (2·15). In addition, even when Λ_n fluctuates, λ_q can be independent of q (see § 3).

$$r_n \simeq \exp(x_0 n)\, r_0 . \tag{2·16}$$

Accordingly near $a=a_c$ there are two time scales $1/\lambda_0$ and $1/|x_0|$.[4] The former characterizes the trajectory instability in the $x_n^{(1)}=x_n^{(2)}$ space ($x_{n+1}^0=f(x_n^0)$), and the latter estimates either the decay time of non-uniformity for $a>a_c$ or the time corresponding to the growing of non-uniformity for $a \lesssim a_c$. In the linear range with respect to r_n, therefore, the dynamics of r_n can be described by only one time scale $1/|x_0|$. Furthermore, since $D=0$, we cannot apply the central limit theorem and $P(z,n)$ does not obey (2·8). Nevertheless, it may still have a peak at $z=x_0 n$, but its width is smaller than $O(\sqrt{n})$ as $n \to \infty$.

The local expansion rate Λ_n, however, does usually strongly depend on the state position x_n^0. This leads to a dispersion of λ_q with a sigmoidal shape.[7),*] Accordingly, the trajectory instability of the uniform chaos can be characterized by an infinite number of time scales continuously lying in the region $1/\lambda_\infty < \tau < 1/\lambda_{-\infty}$ with the assumption $\lambda_{-\infty}>0$, and the power q turns out to be a parameter to single out the time scale $1/\lambda_q$. The Lyapunov exponent λ_0 is just one of them. As a result, we expect that near $a=a_c$ the temporal evolution of the difference r_n (Eq. (1·17b)) has an infinitely many time-scales (Eq. (2·14)), as far as r_n is sufficiently small so that $O(r_n^2)$ can be neglected. This is the crucial difference from the case where λ_q has no dispersion.

In the following sections, utilizing the logistic parabolla

$$f(x)=ax(1-x) , \tag{2·17}$$

we will study (1·18) and (1·19) for a slightly below a_c in connection with the fluctuation effect of local expansion rates on the statistical characteristics of the temporal evolution of the difference v_n or r_n. Typically, we consider two cases, (i) $a=4$ (Case A), where λ_q has no dispersion, and (ii) $a=3.8$ (Case B), where λ_q has a sufficient dispersion.

§ 3. Intermittency in Case A

The uniform chaos is governed by $x_{n+1}^0=4x_n^0(1-x_n^0)$. Clearly the local expansion rate depends on x_n^0 as $\Lambda_n=\ln|4(1-2x_n^0)|$. However, since this system can be transformed into the tent map $\tilde{x}_{n+1}^0=2\tilde{x}_n^0$ for $0 \leqq \tilde{x}_n^0 < 1/2$ and $2-2\tilde{x}_n^0$ for $1/2 \leqq \tilde{x}_n^0 < 1$, λ_q has no dispersion,[**]

$$\lambda_q=\lambda_0=\ln 2 . \tag{3·1}$$

The similarity exponent numerically calculated is shown in Fig. 1(a), which ensures the validity of (3·1).

Near $a=a_c$ we calculated the largest Lyapunov exponent $\lambda^{(1)}$ and the second Lyapunov exponent $\lambda^{(2)}$ of (1·18) and (1·19), (Fig. 2). One clearly observes that the

*) If (2·8) holds for $|z| \leqq \infty$, we obtain $\lambda_q=\lambda_0+Dq$. This is equivalent to that Λ_n is purely the Gaussian.[7] However Λ_n is far from the Gaussian, and so λ_q is usually bounded, $(-\infty<\lambda_{-\infty}<\lambda_q<\lambda_\infty<\infty)$. This means that the asymptotic form (2·8) breaks down in its tail regions.[7] More precisely speaking, the expression (2·8) is valid only for $|z-x_0 n| \lesssim O(\sqrt{Dn})$. Particularly, near $z \simeq x_{\pm\infty} n$, $P(z, n)$ have intensities of the order $\exp(-n/\tau_\pm)$,[7] where τ_+ and τ_- are the characteristic times specifying the dynamics of $\sum_{j=0}^{n-1}\Lambda_j$.

**) The λ_q for the above tent map is ln2, independently of q. Recall that λ_q is invariant under a one-to-one transformation of the dynamics $x_{n+1}=f(x_n)$.

transition occurs at a_c. The system has no hysteresis at $a=a_c$. For $a>a_c$, we find $\lambda^{(1)} \simeq \lambda_0$ and $\lambda^{(2)} \simeq a_c - a (<0)$. On the other hand, for $a<a_c$

$$\lambda^{(1)} - \lambda_0 \simeq -k_1(a_c - a), \qquad \lambda^{(2)} \simeq k_2(a_c - a)^2, \tag{3·2}$$

where $k_1 \simeq 1.0$ and $k_2 \simeq 3.5$.

The typical temporal evolution of r_n for $a \lesssim a_c$ is shown in Fig. 3. Its temporal evolution turns out to consist of two typical processes:[4] (i) The exponential growing region where the envelope of r_n obeys

$$r_n \simeq e^{\beta n} r_0, \qquad (\beta > 0) \tag{3·3}$$

with a certain constant β and (ii) a sudden diminishment of r_n. Such behaviors can be understood as follows. Assume that r_0 is sufficiently small. As far as the $O(r_n^2)$ term is neglected, r_n is given by $r_n \simeq \exp(z_n) r_0$ with $z_n = \sum_{j=0}^{n-1} \{\ln|f'(\bar{x}_j)| - a\}$, where $\bar{x}_n$ obeys $\bar{x}_{n+1} = f(\bar{x}_n) + O(r_n^2)$. For an appropriately large n for which $O(r_n^2)$ is neglected, z_n can be replaced by $x_0 n + o(n)$, because the fluctuation of $\ln|f'(\bar{x}_j)|$ does not accumulate so as to give the dispersion in λ_q. Therefore we obtain $r_n \simeq \exp(x_0 n) r_0$. This explains the exponential growing (3·3) under the replacement

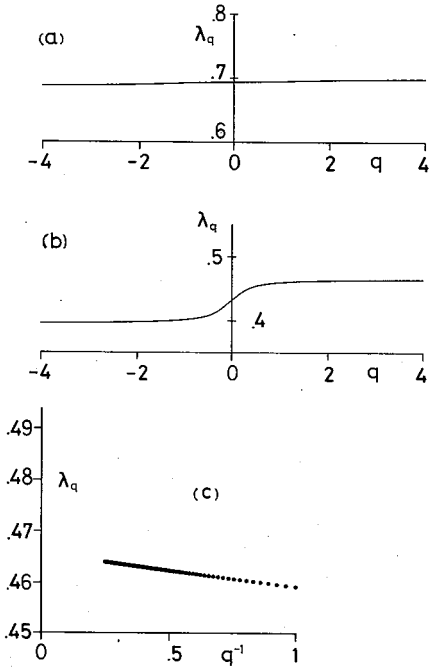

Fig. 1. Similarity exponents numerically obtained for $x_{n+1} = a x_n (1 - x_n)$, where $a=4$(a) and 3.8(b). Numerically λ_q has been calculated by $\lambda_q = q^{-1} n^{-1} \ln \langle \exp(q \sum_{j=0}^{n-1} \Lambda_j) \rangle$, where $\langle \cdots \rangle$ is the average over different initial conditions, and we put $n=1000$. Neglecting numerical error, we find $\lambda_q = \ln 2 = 0.693147\cdots$ for $a=4$. For $a=3.8$, λ_q shows a dispersion ($\lambda_0 = 0.4323\cdots$). Figure 1(c) is the $q^{-1} - \lambda_q$ plot for $a=3.8$. Extrapolating it to $q^{-1}=0$, one can determine $\lambda_\infty (\simeq 0.466)$.

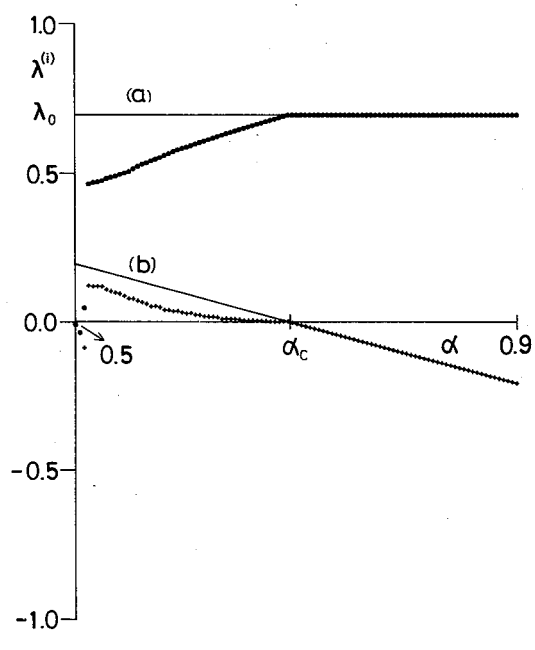

Fig. 2. Numemical results for the largest Lyapunov exponent $\lambda^{(1)}(\cdot)$ and the second Lyapunov exponent $\lambda^{(2)}(+)$ for the coupled-map system (1·14) with $f(x) = 4x(1-x)$. Each value was calculated by averaging over 10^5 iterations. Two straight lines a and b are $\lambda^{(1)} = \lambda_0$ and $\lambda^{(2)} = a_c - a$, respectively, which are valid only for $a \geqq a_c$.

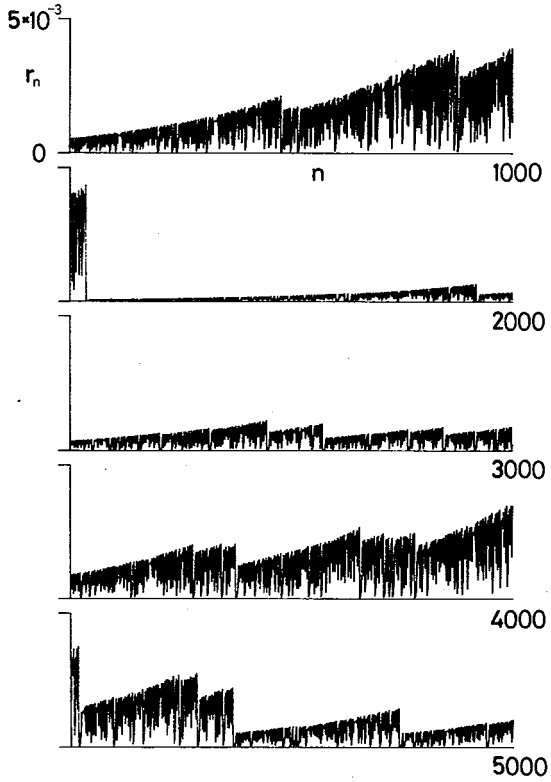

Fig. 3. Typical temporal evolution of r_n in Case A after sufficiently long initial steps. The parameter is $\alpha=0.69$.

$$\beta=x_0\,. \tag{3·4}$$*)

As n increases, however, the nonlinear term with respect to r_n becomes crucial, leading to a sudden reduction of r_n. Repeating this process, r_n shows the temporal evolution as in Fig. 3, being steady.

Although the above characteristic evolution makes us recall the similarity to the tangential instability,[8),9)] the crucial difference is as follows. Near the tangential intermittency point x_*, the deviation from it may obey $dr_n/dn\sim\varepsilon+br_n^{\zeta}$, where $b>0$ and $\varepsilon(0<\varepsilon\ll1)$, is the control parameter, ζ being the order of the map near x_*. For $\zeta=2$, this can be solved as $r_n\sim\sqrt{\varepsilon/b}\tan(\sqrt{b\varepsilon}\,n)$,[8),9)] if $r_0=0$ and $n<\pi/2\sqrt{b\varepsilon}$. This does not exhibit an exponential growing.**) Hereafter the present intermittency will be called *Type A intermittency*.***)

In order to study the statistical properties of r_n, we have calculated the probability density $P_L(r)$ for r_n, which is normalized in the range $0\leqq r\leqq L$, where L is a certain scale (Fig. 4). For a sufficiently small L, $P_L(r)$ seems to obey the power law[4)]

$$P_L(r)\simeq cr^{-1}(r/L)^{\eta}\propto r^{-1+\eta}\,, \tag{3·5}$$

where we numerically obtain $\eta\simeq0.8\simeq c$. Such behavior seems also to be different from the tangential intermittency. The power law behavior (3·5) seems to suggest the existence of a certain kind of a similarity law (Appendix B).

Since r_n has only one characteristic time $1/x_0$, the power spectrum of r_n can be approximated for $x_0\to0$ and $\omega\to0$ by the Lorentzian

$$S(\omega)\simeq2C_0x_0^{-1}L(\omega/x_0) \tag{3·6}$$

with $C_0=\langle r_0^2\rangle-\langle r_0\rangle^2$ and

$$L(y)=\frac{1}{1+y^2} \tag{3·7}$$

(see Appendix C). As is shown in Fig. 5, the theoretical curve (3·6) explains the

*) In fact the value $x_0\fallingdotseq0.003$ for $\alpha=0.69$ coincides with the growth rate β estimated from Fig. 3.

**) If $\zeta=1$, then r_n exhibits the exponential growing, $r_n\propto b^n$ because $b>1$.

***) As will be shown later, the power spectrum of the present r_n exhibits the Lorentzian form rather than a $1/\omega$ form.[8)]

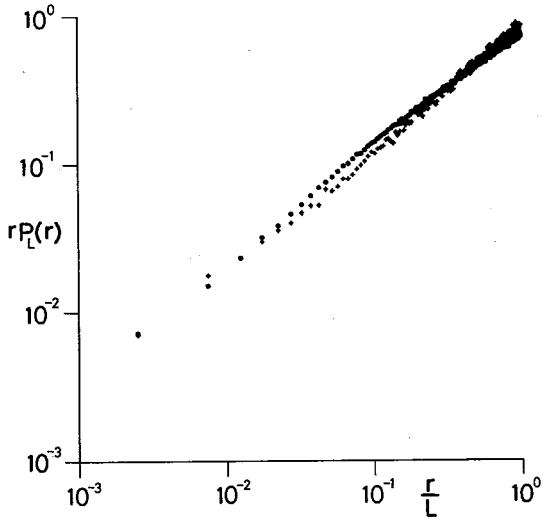

Fig. 4. The probability density $P_L(r)$ for r_n in Case A, where $\alpha=0.691$ and L is chosen as $L=2\times10^{-4}(\cdot)$ and $2\times10^{-5}(+)$.

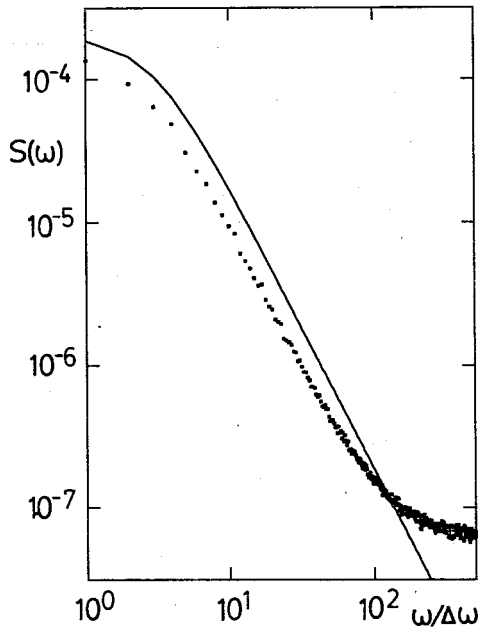

Fig. 5. The comparison of the numerical power spectrum (■) for r_n with the theoretical one (solid line) given by (3·6), where we have used the value $C_0=1.20\times10^{-7}$ numerically obtained. The parameters are $a=4$ and $\alpha=0.692$. The numerical power spectrum was obtained by averaging 500 power spectra each of which was calculated by FFT for the sampling length 2^{14} ($\Delta\omega=2\pi/2^{14}$).

numerical results fairly in a good manner. It is worthwhile to note that the approximation (3·6) is consistent with the fact that there is only one characteristic time scale for r_n near $\alpha=\alpha_c$(§ 2), at least as far as the long time dynamics is concerned.

§ 4. Intermittency in Case B

Second, we will adopt the logistic parabolla $f(x)=3.8x(1-x)$. We numerically find $\lambda_0=0.4323\cdots$. The similarity exponent is shown in Fig. 1(b). In contrast to Case A, the present λ_q exhibits a sufficient dispersion. This means that the trajectory instability of (1:2) is characterized by an infinite number of growth rates lying between $\lambda_{-\infty}(\simeq0.4)$ and $\lambda_\infty(\simeq0.47)$ (see § 2). Furthermore, for a large q, λ_q can be expanded as $\lambda_q\simeq\lambda_\infty-\tau_+^{-1}q^{-1}$,[7] where $\tau_+\simeq150$ (Fig. 1(c)).

Near $\alpha=\alpha_c$, we have calculated the Lyapunov exponents (Fig. 6). The transition does not follow a hysteresis. For $\alpha>\alpha_c$, we obtain $\lambda^{(1)}\simeq\lambda_0$ and $\lambda^{(2)}\simeq\alpha_c-\alpha(<0)$. On the other hand, for $\alpha<\alpha_c$

$$\lambda^{(1)}-\lambda_0\simeq-k_1(\alpha_c-\alpha)\,,\qquad \lambda^{(2)}\simeq k_2(\alpha_c-\alpha)\,, \tag{4·1}$$

where $k_1\simeq1.8$ and $k_2\simeq1.5$. The critical behavior of present $\lambda^{(2)}$ for $\alpha\lesssim\alpha_c$ is different from

that in Case A (Eq. (3·2)).

The temporal evolution of v_n after sufficiently long initial steps is drawn in Figs. 7(a) ~(e). Clearly v_n exhibits a highly intermittent characteristics. The present intermittency differs from the tangential intermittency and also from Type A intermittency, but is characterized by alternative generation of quiescent regions ($r_n \simeq 0$) and bursts having considerably large values of r_n and being located in very narrow time domains.[4] This new type intermittency will be called *Type B intermittency*.

Let us turn to the reason why such highly intermittent behaviors as in Figs. 7(a)~(e) are observed. Assume that r_n starts initially with a sufficiently small r_0. In the region where $O(r_n^2)$ can be neglected, we get $r_n \simeq \exp(z_n) r_0$ with $z_n \equiv \sum_{j=0}^{n-1} \{\ln|f'(\bar{x}_j)| - a\}$. In contrast to Case A, the present z_n strongly fluctuates from $\chi_{-\infty} n$ to $\chi_{\infty} n$ by ignoring terms of $o(n)$. Namely, z_n widely spreads asymptotically with the normal form. If we put $z_n = \gamma n + o(n)$, γ is a stochastic variable lying $\chi_{-\infty} < \gamma < \chi_{\infty}$. Since $a \lesssim a_c$, one obtains $\chi_{-\infty} < 0 < \chi_0$. Namely, γ can be either positive or negative. If γ remains negative in a certain

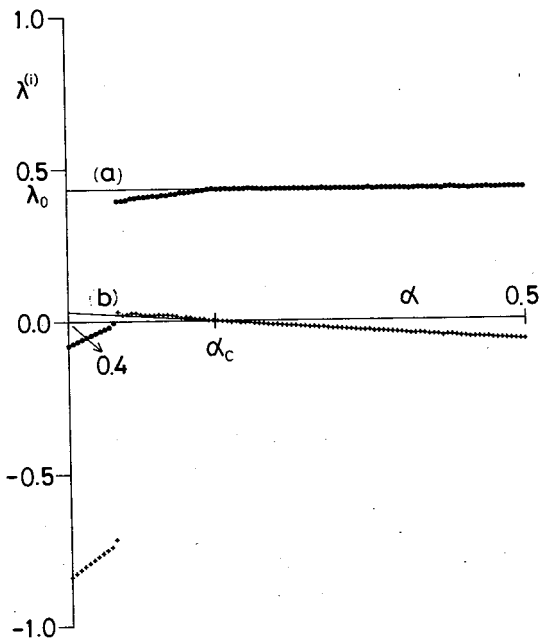

Fig. 6. Numerical result for the largest Lyapunov exponent $\lambda^{(1)}(\cdot)$ and the second Lyapunov exponent $\lambda^{(2)}(+)$ for the coupled-map system (1·14) with $f(x) = 3.8x(1-x)$. Each value was obtained by averaging over 10^5 iterations. Two straight lines are $\lambda^{(1)} = \lambda_0$ and $\lambda^{(2)} = a_c - a$, respectively, which are valid only for $a \geqq a_c$.

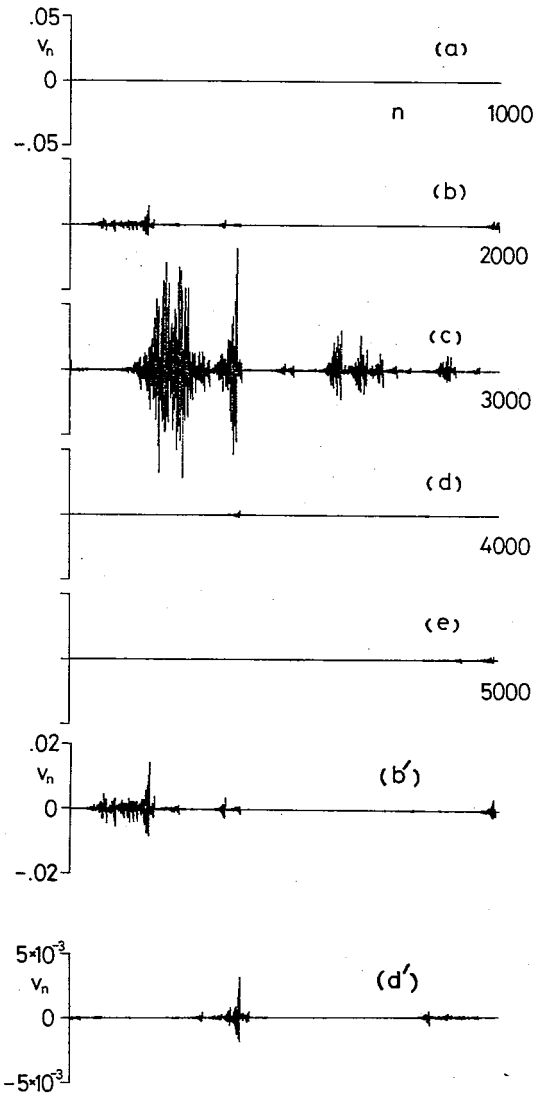

Fig. 7. Typical temporal evolution of v_n in Case B after sufficiently long initial steps (a)~(e). The parameter is $a = 0.43$. (b') ((d')) is the enlargement of Fig. 7(b) ((d)). They exhibit the self-similarity of the temporal evolution.

temporal region, r_n shrinks, and one observes quiescent regions. If γ happens to be positive, r_n starts to grow, leading to the ignition of a burst.

Furthermore, we add the following remark. In Figs. 7(b), (d) and (e), there are small oscillations (bursts) temporally localized. Figure 7(b′) (7(d′)) is the enlargement of Fig. 7(b) (7(d)). Apparently they have similar structures as in Fig. 7(c). Thus we might say that Type B intermittency is characterized by the self-similar temporal evolution of v_n in this sense.

We have calculated the probability density $P_L(r)$ (Fig. 8). For a sufficiently small L, $P_L(r)$ seems to obey the power law

$$P_L(r) \propto r^{-1+\eta}, \qquad (\eta \simeq O(10^{-2})) \tag{4·2}$$

for $r/L > h(=1/200)$. The exponent η is extremely small and we cannot give a precise value. $P_L(r)$ has a remarkable deviation from the law (4·2) for an extremely small $r(r/L < h)$. The origin of this deviation may be understood as follows. Since (4·2) is not integrable if we put $\eta=0$, for any tiny subunit $\Delta_M(=L/M, M$ being the number of subspaces) the probability integrated from zero to Δ_M diverges. In numerical calculations, however, it always remains finite but is outstandingly large. It seems that the deviation for $r/L < h$ suggests the law $P_L(r) \propto r^{-1}$.

The power spectrum for r_n numerically obtained is shown in Fig. 9. As was reported

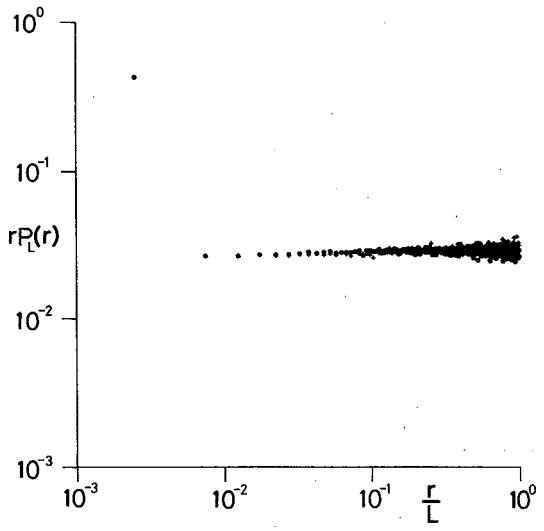

Fig. 8. The probability density $P_L(r)$ for r_n in Case B for $a=0.431$, where L is chosen as $L=2\times10^{-6}(\cdot)$ and $2\times10^{-7}(+)$. Except the first datum, $P_L(r)$ is close to the inverse power law $(\propto r^{-1})$.

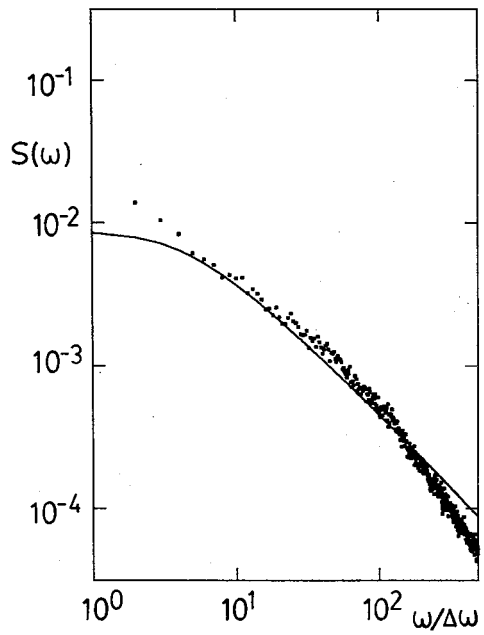

Fig. 9. The comparison of the numerical power spectrum (■) of r_n for $a=0.431$ with the theoretical curve (solid line) given by (4·3). Here we used the value $C_0=4.20\times10^{-5}$ numerically obtained. The numerical power spectrum was obtained by averaging 500 power spectra each of which was calculated by FFT for the sampling length 2^{14} $(\Delta\omega=2\pi/2^{14})$. The numerical power spectrum is close to a ω^{-1} form for $\omega \gg \varkappa_0$.

previously,[4] the present power spectrum is far from the single Lorentzian (3·6), and is rather close to the ω^{-1} form in a certain frequency region. This means that the r_n dynamics cannot be characterized by the single time $1/\varkappa_0$, which is consistent with the multi time-scales situation, as was discussed in the earlier part of this section (see also §2). Noting that there exist an infinite number of damping rates continuously spread, we propose a power spectrum

$$S(\omega)\simeq\frac{2C_0}{\varkappa_0\ln(2/\varkappa_0)}T\left(\frac{\omega}{\varkappa_0}\right) \tag{4·3}$$

for $\varkappa_0\to 0$ and $\omega\to 0$, where

$$T(y)=\frac{1}{y}\left\{\frac{\pi}{2}-\arctan\left(\frac{1}{y}\right)\right\} \tag{4·4}$$

(see Appendix D). Equation (4·3) seems to be fairly in a good agreement with the numerical result except $\omega/\Delta\omega\lesssim 4$. By making use of the asymptotic behaviors of $T(y)$, (4·3) becomes

$$\frac{S(\omega)}{2C_0/\varkappa_0\ln(2/\varkappa_0)}\simeq 1-\frac{1}{3}\left(\frac{\omega}{\varkappa_0}\right)^2+\cdots, \quad (\omega\ll\varkappa_0) \tag{4·5a}$$

$$\simeq\frac{\pi}{2}\cdot\frac{\varkappa_0}{\omega}\left(1-\frac{2}{\pi}\cdot\frac{\varkappa_0}{\omega}+\cdots\right). \quad (\omega\gg\varkappa_0) \tag{4·5b}$$

For $\omega\gg\varkappa_0$ the power spectrum exhibits the ω^{-1} law. This is a crucial difference from that in Case A ($S(\omega)\propto(\varkappa_0/\omega)^2$ for $\omega\gg\varkappa_0$).

§ 5. Summary and remarks

We have developed a fluctuation theory on the stability of the synchronized chaos of the coupled system (1·14). It was shown that the system undergoes the transition from the uniform chaos to the non-uniform chaos as the coupling strength a is gradually decreased. The transition occurs when the second Lyapunov exponent in Ψ_{unif} crosses zero from negative to positive, i.e., the transition point a_c is determined by the largest Lyapunov exponent in Ψ_{unif}.

For a slightly below a_c, the system exhibits an intermittent behavior, whose characteristics is closely related with the statistical properties of local expansion rates of the isolated system $x_{n+1}=f(x_n)$. Namely, when the similarity exponent λ_q has no dispersion, the intermittency is characterized by alternative generation of the exponential growing of r_n and its sudden diminishment (Type A intermittency). On the other hand, when λ_q has a sufficient dispersion, the intermittency is different from the above and consists of quiescent regions abruptly inserted by temporally highly localized bursts (Type B intermittency). In both cases, the probability density for r_n exhibits the power law behavior

$$P_L(r)\propto r^{-1+\eta} \tag{5·1}$$

for sufficiently small r, and the power spectrum satisfies the scaling law

$$\frac{S(\omega)}{2C_0}\simeq\varkappa_0^{-1}\Omega\left(\frac{\omega}{\varkappa_0}\right) \tag{5·2}$$

for $x_0 \to 0$ and $\omega \to 0$, if we neglect the factor of order $\ln x_0^{-1}$. When λ_q has no dispersion, the exponent η is $O(1)$ and the scaling function $\Omega(y)$ is well approximated by the Lorentzian (3·7). On the other hand, when λ_q has a sufficient dispersion, η is very close to zero, and $\Omega(y)$ is far from the Lorentzian (Eq. (4·4)), having the y^{-1} form for $y \gg 1$, which corresponds to the ω^{-1} law of the power spectrum for $\omega \gg x_0$.

Since λ_q for an arbitrary system $x_{n+1}=f(x_n)$ generally more and less has a dispersion if x_n is chaotic, the intermittency observed for $a \lesssim a_c$ is expected to exhibit characteristics the same as Type B intermittency even if the dispersion of λ_q is weak. We have calculated another coupled logistic parabolla system with $a=3.65$ ($\lambda_0 \simeq 0.255\cdots$). The quantity $\Delta = \lambda_\infty - \lambda_{-\infty}$ measures the strength of the dispersion of λ_q. For $a=3.8$, $\Delta \simeq 0.07$. However, for $a=3.65$, Δ is smaller than 0.07 ($\simeq 0.04$). For the x_0 value of the same order as in §§ 3 and 4, the temporal evolution of r_n seems to exhibit a mixed characteristics of Type A and Type B intermittencies. The exponent η is between 0 and 0.8. We numerically found that as a is approached to a_c, η tends to vanish as

$$\eta \propto a_c - a \,. \tag{5·3}^{*)}$$

Since Type B intermittency is characterized by an extremely small value of η, we might say that even when the dispersion of λ_q is weak, we can observe Type B intermittency as the system approaches a_c. This suggests the existence of the crossover point a_* from Type A intermittency to Type B intermittency as a approaches a_c from below.

The essential point to explain the ω^{-1}-like power spectrum in Type B intermittency was based on the existence of an infinite number of time-scales for r_n. It should be noted that this situation has a close connection with the introduction of the distribution function for durations among bursts near the onset of tangential intermittency.[10)~12)]

Recently the intermittent characteristics similar to Type B intermittency has been found by Tomita and Sakaguchi[13)] for the temporal evolution of X_n in the coupled system

$$X_{n+1} = A Y_n X_n (1 - X_n) \,, \tag{5·4a}$$

$$Y_{n+1} = B Y_n (1 - Y_n) \,, \tag{5·4b}$$

where A and B are close to 4. Particularly, for $A=B=4$, they have found a ω^{-1}-like power spectrum for X_n. From a standpoint of the stability of the fixed point $X_n=0$, the above system can be studied in a similar way as in the present paper. Detailed analyses will be reported elsewhere.

Finally, we note that Kaneko has reported an intermittency phenomenon in his coupled-map lattice system.[14)] His intermittency is rather spatial than temporal. It may be an important task to clarify the interrelation between the temporal and spatial intermittencies.

Acknowledgements

The authors thank Professor H. Mori for continuous encouragement and valuable discussions. This study was partially supported by the Scientific Research Fund of the Ministry of Education, Science and Culture.

*) For $a=4$, η is numerically shown to remain finite ($\simeq 0.8$) even a approaches a_c.

Appendix A

Let us start with the perturbation equation of (1·5) around the synchronized motion x_n^0, ($u_n(\boldsymbol{\xi}) \equiv x_n(\boldsymbol{\xi}) - x_n^0$),

$$u_{n+1}(\boldsymbol{\xi}) = f'(x_n^0)\, \hat{\phi}_{-i\nabla}\, u_n(\boldsymbol{\xi}) , \tag{A·1}$$

where $x_{n+1}^0 = f(x_n^0)$. The Fourier transform $\hat{u}_{n,\boldsymbol{k}}$ of $u_n(\boldsymbol{\xi})$ obeys

$$\hat{u}_{n+1,\boldsymbol{k}} = f'(x_n^0)\, \hat{\phi}_{\boldsymbol{k}}\, \hat{u}_{n,\boldsymbol{k}} . \tag{A·2}$$

The stability of Ψ_{unif} can be discussed with the exponent $\Lambda_{\boldsymbol{k}}$ for the wavenumber $\boldsymbol{k}$, defined by

$$\Lambda_{\boldsymbol{k}} = \lambda_0 + \ln|\hat{\phi}_{\boldsymbol{k}}| , \tag{A·3}$$

where λ_0 is the Lyapunov exponent of $x_{n+1}^0 = f(x_n^0)$ (Eq. (2·5)). Here we have used (1·7).

If $\Lambda_{\boldsymbol{k}} < 0 (> 0)$ for all (certain) $\boldsymbol{k}$, fluctuations around the uniform oscillation Ψ_{unif} are linearly stable (unstable). Since the system (1·4) or (1·5) is regarded as the dynamical equation governing the macroscopic motion, we can assume that the microscopic degrees of freedom have been eliminated under the assumption that they are always stable irrespective of macroscopic motion. This gives the condition that $\Lambda_{\boldsymbol{k}}$ should be negative, if $|\boldsymbol{k}|$ is sufficiently large. Particularly, for (1·9) we obtain [1),3)]

$$\Lambda_{\boldsymbol{k}} = \lambda_0 - a\boldsymbol{k}^2 , \tag{A·4}$$

which satisfies the above condition. Equation (A·4) is a monotonously decreasing function of $|\boldsymbol{k}|$ and its sign changes at $|\boldsymbol{k}| = \sqrt{\lambda_0/a}$ from positive to negative, if Ψ_{unif} is chaotic, ($\lambda_0 > 0$). On the other hand, if Ψ_{unif} is periodic ($\lambda_0 < 0$), then $\Lambda_{\boldsymbol{k}}$ is always negative. This means that the uniform periodic oscillation is stable[1)~3)] against spatial non-homogeneous fluctuations.

Let us turn to (1·18) and (1·19). When the non-uniformity is weak, they can be expanded in v_n (Eq. (1·17b)) as

$$\bar{x}_{n+1} = f(\bar{x}_n) + \frac{f''(\bar{x}_n)}{2} v_n^2 + O(v_n^4) , \tag{A·5a}$$

$$v_{n+1} = e^{-a}\{f'(\bar{x}_n) v_n + O(v_n^3)\} . \tag{A·5b}$$

Hereafter we will show that when the uniform chaos is weak and (1·4) in one dimensional space can be described by the three mode truncation, (1·4) is equivalent to (A·5), and so, is essentially the same as (1·14). Let the system be on a line with the length l under the periodic boundary condition. We divide $x_n(\xi)$ as

$$x_n(\xi) = \bar{x}_n + u_n(\xi) , \tag{A·6}$$

where $\bar{x}_n$ is the spatial average of $x_n(\xi)$ ($\bar{x}_n = l^{-1}\int_0^l x_n(\xi)\, d\xi$), and $u_n(\xi)$ is the fluctuation. By introducing the Fourier transform

$$\hat{u}_{n,k} = \int u_n(\xi) e^{-ik\xi} d\xi , \qquad (u_n(\xi) = \int e^{ik\xi} \hat{u}_{n,k} dk/2\pi) \tag{A·7}$$

(1·4) can be written as

$$\bar{x}_{n+1}+\frac{1}{l}\sum_k \hat{u}_{n+1,k}e^{ik\xi}=f(\bar{x}_n)+f'(\bar{x}_n)\frac{1}{l}\sum_k \hat{\phi}_k \hat{u}_{n,k}e^{ik\xi}$$

$$+\frac{f''(\bar{x}_n)}{2l^2}\sum_{k_1}\sum_{k_2}\hat{\phi}_{k_1+k_2}\hat{u}_{n,k_1}\hat{u}_{n,k_2}e^{i(k_1+k_2)\xi}+O(\hat{u}^3)\,, \tag{A·8}$$

where $\sum_k\cdots=(l/2\pi)\int dk\cdots$. Now we assume that λ_0 is appropriately small and (A·8) can be approximated by three modes with wavenumbers $k=-Q, 0, Q$ $(Q>0)$. The uniform mode $(k=0)$ turns out to obey

$$\bar{x}_{n+1}\simeq f(\bar{x}_n)+\frac{f''(\bar{x}_n)}{l^2}|\hat{u}_{n,Q}|^2\,, \tag{A·9a}$$

where we have used $\hat{u}_{n,0}=0$. Comparing the Fourier coefficients for $k=Q$ of both hand sides of (A·8), we get

$$\hat{u}_{n+1,Q}=\hat{\phi}_Q\{f'(\bar{x}_n)\,\hat{u}_{n,Q}+O(\hat{u}^3)\}\,. \tag{A·9b}$$

Under the replacement

$$\hat{\phi}_Q=e^{-\alpha+i\theta}\,,\qquad \hat{u}_{n,Q}=\frac{l}{\sqrt{2}}v_n e^{i\theta}\,, \tag{A·10}$$

v_n being chosen as a real number, (A·9a) and (A·9b) are equivalent to (A·5a) and (A·5b), respectively provided that $O(v_n{}^3)$ are neglected.

Appendix B

—— *The Power Law Behavior of* $P_L(r)$ ——

Let us consider a set $R\equiv\{r_j, j=1, 2, 3, \cdots, M\}$, where M is taken to be sufficiently large. We divide R into two subsets $R(L)$ and $R'(L)$. Here an element of $R_j(j=1, 2, 3, \cdots, N)$ of $R(L)$ satisfies $R_j\leqq L$ and an element R_l' $(l=1, 2, 3, \cdots, M-N)$ of $R'(L)$ satisfies $R_l'>L$, where $L(\ll 1)$ is an arbitrary constant, and N and $M-N$ are assumed to be sufficiently large.

The probability density $P_L(r)$ is calculated with the subset $R(L)$ by

$$P_L(r)=\lim_{M\to\infty}\frac{1}{N}\sum_{j=1}^{N}\delta(R_j-r)\,.\quad (0\leqq r\leqq L) \tag{B·1}$$

By putting $R_j=L\tilde{R}_j$, (B·1) can be rewritten as

$$P_L(r)=\frac{1}{r}g\left(\frac{r}{L}\right), \tag{B·2}$$

where

$$g(\theta)\equiv\lim_{M\to\infty}\frac{1}{N}\sum_{j=1}^{N}\delta(\ln\tilde{R}_j-\ln\theta) \tag{B·3}$$

is independent of L.

We define the scale

$$r^{(l)}=2^{-l}L\,.\quad (l=0, 1, 2, \cdots) \tag{B·4}$$

Let A_l be the average of r taken over $0 \leqq r \leqq r^{(l)}$,

$$A_l = \frac{1}{2^{-l}} \int_0^{r(l)} r P_L(r)\, dr \,. \tag{B·5}$$

Under the similarity assumption, the ratio

$$\frac{A_{l+1}}{A_l} = 2^{-\eta} \tag{B·6}$$

is assumed to be independent of l and η is assumed to be non-negative. If $\eta \neq 0$, then the comparison of (B·6) with (B·2) yields

$$g(\theta) = \eta \theta^{\eta} \,. \tag{B·7}$$

We obtain

$$P_L(r) = \eta r^{-1} (r/L)^{\eta} \,. \tag{B·8}$$

On the other hand, if $\eta = 0$, then $g(\theta)$ is independent of θ, leading to

$$P_L(r) \propto r^{-1} \,. \tag{B·9}$$

This is not normalizable at $r = 0$.

Appendix C

—— *Derivation of* (3·6) ——

As was discussed in § 3, the temporal evolution of r_n in Case A consists of two characteristic processes, the exponential growing with the rate $\varkappa_0$ and its sudden diminishment. With this observation we propose a modeled stochastic process,

$$\delta r_{n+1} = e^{\varkappa_0} \delta r_n + R_n \,. \qquad (\varkappa_0 > 0,\ \delta r_n \equiv r_n - \langle r_n \rangle) \tag{C·1}$$

R_n is the random force ($\langle R_n \rangle = 0$) caused by the nonlinear effect of δr_n and satisfies

$$\langle R_n R_0 \rangle = I \delta_{n0} \,, \tag{C·2}$$

where I is the intensity of R_n, and $\langle \cdots \rangle$ is the average over the ensemble for the random force. In the temporal region where r_n exponentially grows, R_n takes almost zero. The exponential growing ceases to continue when R_n acts, leading to a sudden diminishment of r_n. As a result, r_n can be steady. Our stochastic model is different from the Ornstein-Uhlenbeck process by the sign of $\varkappa_0$, where R_n acts so as to excite the deviation from the average $\langle r_n \rangle$.

Solving (C·1) yields

$$\delta r_n - e^{\varkappa_0 n} \delta r_0 = \sum_{s=0}^{n-1} e^{\varkappa_0 (n-1-s)} R_s \,. \tag{C·3}$$

Taking the square of (C·3) and the average, we get, for $n \geqq 0$,

$$C_0 (1 + e^{2\varkappa_0 n}) - 2 e^{\varkappa_0 n} C_n = I (e^{2\varkappa_0 n} - 1) / (e^{2\varkappa_0} - 1) \,, \tag{C·4}$$

where $C_n = \langle \delta r_n \delta r_0 \rangle$ is the double time correlation function. Since r_n is steady, C_n should vanish as $n \to \infty$, which requires the equality

$$C_0 = I / (e^{2\varkappa_0} - 1) \,. \tag{C·5}$$

This is nothing but the fluctuation-dissipation theorem, which ensures the balance between the growing of r_n and the action of the random force, i.e., ensures the stationality of the process $\{r_n\}$. The insertion of (C·5) into (C·4) leads to

$$C_n = C_0 e^{-\kappa_0 n} \tag{C·6}$$

for $n \geqq 0$. Substituting (C·6) into $S(\omega) = \sum_{n=-\infty}^{\infty} C_{|n|} e^{i\omega n}$ gives the power spectrum[4]

$$S(\omega) = \frac{C_0}{2} \cdot \frac{\sinh(\kappa_0)}{\sinh^2(\kappa_0/2) + \sin^2(\omega/2)} . \tag{C·7}$$

In the limit $\kappa_0 \to 0$ and $\omega \to 0$, this becomes (3·6).

Since the random force R_n acts so as to make δr_n steady, there is still a correlation between δr_0 and R_n as

$$\langle R_n \delta r_0 \rangle = 0 , \qquad (n \leqq -1) \tag{C·8a}$$

$$= -2C_0 \sinh(\kappa_0) e^{-\kappa_0 n} . \qquad (n \geqq 0) \tag{C·8b}$$

This is again different from the assumption made in the Ornstein-Uhlenbeck process ($\langle R_n \delta r_0 \rangle = 0$ for $n \geqq 0$).

Appendix D

— Derivation of (4·3) —

Noting that in Case B there are a continuously infinite number of damping rates near $\alpha = \alpha_c$, we assume that the power spectrum of r_n for $\alpha \lesssim \alpha_c$ is given by the superposition of "Lorentzians",

$$S(\omega) = \frac{C_0}{2} \int_0^{\infty} g(\chi) \frac{\sinh(\chi)}{\sinh^2(\chi/2) + \sin^2(\omega/2)} d\chi . \tag{D·1}$$

Here $g(\chi)$ is the density of mode with the decay rate χ and is assumed to vanish for $\chi < \Gamma_l$ and $\chi > \Gamma_u (\Gamma_u > \Gamma_l > 0)$. We further assume that Γ_l is small for $\alpha \lesssim \alpha_c$ and vanishes at α_c. Since one typical characteristic inverse time near $\alpha = \alpha_c$ is κ_0, one may put $\Gamma_l \simeq \kappa_0$. On the other hand, Γ_u is assumed to be $O(\kappa_0^0)$ near $\alpha = \alpha_c$.

For a sufficiently low ω, the most dominant contribution to $S(\omega)$ comes from sufficiently small χ, if $g(\chi)$ smoothly depends on χ. Assuming that the most dominant part of $g(\chi)$ for small χ is proportional to the "correlation time" $(=1/\chi)$, we assume that $g(\chi) \propto 1/\sinh(\chi)$, which is consistent with $g(\chi) \propto 1/\chi$ for small χ. Since this function rapidly approaches zero as χ increases, large χ modes give less contribution to $S(\omega)$. This allows us to replace Γ_u by ∞. Then (D·1) becomes

$$S(\omega) \simeq BC_0 \int_{\kappa_0}^{\infty} \frac{d\chi}{\sinh^2(\chi/2) + \sin^2(\omega/2)} . \tag{D·2}$$

Here B is determined by the sum-rule $\int_{-\pi}^{\pi} S(\omega)\, d\omega = 2\pi C_0$ as

$$B = 1/2 \ln \coth(\kappa_0/2) . \tag{D·3}$$

Carrying out the integration in (D·2), we obtain

$$S(\omega) \simeq \frac{4BC_0}{\sin|\omega|} \left[\frac{\pi}{2} - \tan^{-1} \left\{ \cot\left(\frac{|\omega|}{2} \right) \tanh\left(\frac{\kappa_0}{2} \right) \right\} \right] . \tag{D·4}$$

In the limit $x_0 \to 0$ and $\omega \to 0$, (D·4) is given by (4·3).

References

1) H. Fujisaka and T. Yamada, Prog. Theor. Phys. **69** (1983), 32 (this is referred to as I).
2) T. Yamada and H. Fujisaka, Prog. Theor. Phys. **70** (1983), 1240 (this is referred to as II).
3) T. Yamada and H. Fujisaka, Prog. Theor. Phys. **72** (1984), 885 (this is referred to as III).
4) H. Fujisaka and T. Yamada, Prog. Theor. Phys. **74** (1985), 918.
5) A. S. Pikovsky, Z. Phys. **B55** (1984), 149.
6) H. Fujisaka, Prog. Theor. Phys. **70** (1983), 1264.
7) H. Fujisaka, Prog. Theor. Phys. **71** (1984), 513.
   H. Fujisaka and M. Inoue, Prog. Theor. Phys. **74** (1985), 20.
8) P. Manneville and Y. Pomeau, Physica **1D** (1980), 219.
9) J. E. Hirsch, B. A. Hubermann and D. J. Scalapino, Phys. Rev. **A25** (1982), 519.
10) Y. Aizawa, Prog. Theor. Phys. Suppl. No. 79 (1984), 96 and references cited therein.
11) I. Procaccia and H. Schuster, Phys. Rev. **A28** (1983), 1210.
12) B. C. So and H. Mori, Prog. Theor. Phys. **72** (1984), 1258.
13) K. Tomita, Prog. Theor. Phys. Suppl. No. 79 (1984), 1.
    H. Sakaguchi and K. Tomita, to be published.
14) K. Kaneko, Prog. Theor. Phys. **72** (1984), 480 and preprint.